EUMETSAT
SAF for Land Surface Analysis
(LSA SAF)

Algorithm Theoretical Basis Document
for
Fire Detection and Monitoring Product
(LSA-29)

Reference Number:	SAF/LAND/IM/ATBD_FD&M/02
Issue/Revision Index:	Issue 0.2
Last Change:	20/10/2009

DOCUMENT SIGNATURE TABLE

	Name	Date	Signature
Prepared by :	Malik Amraoui and Carlos C. DaCamara		
Approved by :	Land SAF Project Manager (IM)		

DOCUMENTATION CHANGE RECORD

Issue / Revision	Date	Description:
Version 0.1	01/06/2009	Version to be presented to PCR
Version 0.2	20/10/2009	Version to be presented to close-out meeting

DISTRIBUTION LIST

Internal Consortium Distribution		
Organisation	**Name**	**No. Copies**
IM	Pedro Viterbo	
IM	Luís Pessanha	
IM	Isabel Trigo	
IDL	Carlos da Camara	
IM	Isabel Monteiro	
IM	Sandra Coelho	
IM	Carla Barroso	
IM	Pedro Diegues	
IM	Teresa Calado	
IM	Benvinda Barbosa	
IM	Ana Veloso	
IMK	Folke-S. Olesen	
IMK	Frank Goettsche	
IMK	Ewa Kabsch	
MF	Jean-Louis Roujean	
MF	Olivier Hautecoeu	
MF	Dominique Carrer	
RMI	Françoise Meulenberghs	
RMI	Arboleda Alirio	
RMI	Nicolas Ghilain	
FMI	Niilo Siljamo	
UV	Joaquin Melia	
UV	F. Javier García Haro	
UV/EOLAB	Fernando Camacho	
UV	Aleixander Verger	

External Distribution		
Organisation	**Name**	**No. Copies**
EUMETSAT	Frédéric Gasiglia	
EUMETSAT	Dominique Faucher	
EUMETSAT	Lorenzo Sarlo	
EUMETSAT	Lothar Schueller	
EDISOFT	Teresa Cardoso	
EDISOFT	Carlos Vicente	
EDISOFT	Cleber Balan	
SKYSOFT	Rui Alves	
SKYSOFT	João Canário	

Steering Group Distribution		
Nominated by:	**Name**	**No. Copies**
IM	Carlos Direitinho Tavares	
EUMETSAT	Lorenzo Sarlo	
EUMETSAT	Yves Govaerts	
EUMETSAT	François Montagner	
STG/AFG (USAM)	Luigi de Leonibus	
MF	François Bouyssel	
RMI	Alexandre Joukoff	
FMI	Tapio Tuomi	

Table of Contents

List of Tables

List of Figures

1. Introduction

1.1. Purpose

Fires are an important and highly variable source of air pollution emissions in many regions of the world and they constitute a significant, if not dominant, factor controlling the interannual variability of the atmospheric composition (Schultz et al., 2008). In this respect, African vegetation fires play a central role in tropical and subtropical atmospheric chemistry and, according to Lacaux et al. (1993), account for 57% of all tropical burning (49% from savanna fires and 8% from forest burns).

Estimates of global direct carbon emissions from wildland fires range from 1428 Tg C/year as estimated by Ito and Penner (2004) to 2771 Tg C/year as calculated by Galanter et al. (2000). According to the 41-year inventory of vegetation fire emissions constructed for the Reanalysis of the Tropospheric chemical composition over the past 40 years project (RETRO), the global total direct carbon emission flux from wildland fire emissions amounts to 2078 Tg C/year (Schultz et al., 2008), the African continent contributing to about one half of the global vegetation fire emissions; 24.75 % for northern Africa and 23.49 % for southern Africa. However, as pointed out by the authors, future versions of the inventory will benefit from ongoing analyses of burned areas based on satellite data.

Several studies have used remotely sensed data to characterize the seasonality of vegetation fires at the continental and global scales (Cahoon et al., 1992; Barbosa et al., 1999; Dwyer et al., 1999, 2000a,b; Schultz 2002; Generoso et al., 2003; Silva et al.; 2003; Tansey et al., 2004a,b; Csiszar et al. 2005; Giglio et al., 2006; Le Page et al., 2008). All of these analyses relied on satellite systems with a frequency of overpass ranging from a minimum of every 3-4 days to a maximum of 4 times per day. In this respect it is worth mentioning the suite of the fire products derived from the Moderate Resolution Imaging Spectrometer (MODIS) sensor, both active fires and burnt area, which are made available by the Fire Information for Resource Management System (FIRMS) at the University of Maryland (USA).This is adequate to depict seasonal patterns extending over a period of a few months, but of limited utility to analyse higher frequency periodicities, such as daily, or even weekly fire cycles. In a recent work, Giglio (2007) characterized the average diurnal fire cycle in 15 regions of the tropics and subtropics using seven years of observations made with the Visible and Infrared Scanner (VIRS) and the MODIS instruments. The author noted that the diurnal cycle was prominent in all these regions, with a maximum of activity in the early-to late-afternoon and typically little or no burning between 00:00 and 08:00 local time.

Quantitative characterization of daily fire cycles is important for several reasons; i) the chemical composition of pyrogenic emissions is affected by dead fuel moisture content (Andreae and Merlet, 2001; Hoffer et al., 2006), which tracks the daily cycle of atmospheric relative humidity, with timelags that are a function of fuel particle size; ii) higher nocturnal atmospheric stability, and especially low-level inversions, may lead to decreased injection heights, thus restricting long-distance dispersal of combustion products (Garstang and Tyson, 1997); iii) the optical depth of biomass burning smoke aerosol displays a strong daily cycle (Smirnov et al., 2002; Eck et al., 2003) and generates radiative impacts that disturb cloud formation and convective rainfall patterns

in the tropics (Rosenfeld, 1999; Smirnov et al., 2002; Andreae et al., 2004). Increasing the temporal resolution of vegetation fire data to hourly or even sub-hourly intervals may therefore contribute towards improving models of environmental processes affected by biomass burning. High frequency fire information is also relevant for civil protection and forest protection activities (Pereira and Govaerts, 2001).

Geostationary meteorological satellite systems provide much higher frequency of observation of the land surface than sun-synchronous systems but, until recently, their spatial and spectral resolutions were sub-optimal for vegetation fire monitoring. Nevertheless, various authors demonstrated the capability of earlier geostationary satellites to detect active fires (Prins and Menzel, 1992, 1994; Prins and Schmetz, 2000) and to estimate burned areas (Boschetti et al., 2003). New possibilities were opened up with the launch in 2002 of Meteosat-8, the first satellite of the Meteosat Second Generation (MSG). Temporal, spatial and spectral characteristics of the MSG series were substantially improved (Schmetz et al., 2002), rendering its satellites very adequate for Earth surface observation, and namely for fire monitoring (Cihlar et al., 1999; Pereira and Govaerts, 2001). The potential of MSG was promptly explored, namely by expanding the scope of previous fire applications of geostationary systems with the goal of quantifying fire intensity and biomass consumption (Roberts et al., 2005; Roberts and Wooster, 2008). In this respect the MPEF FIR product of EUMETSAT for thermal anomalies detection, currently disseminated via EUMETCast is also worth mentioning.

Exploitation of the MSG potential is however particularly suitable in the framework of the SAF on Land Surface analysis (LSA SAF) that is part of the Satellite Application Facility (SAF) Network (DaCamara, 2006). The aim of the LSA SAF is to take full advantage of remotely sensed data available from EUMETSAT sensors to describe/derive land surface properties/variables. For instance, the LSA SAF products are related with physical and biophysical properties of the land surfaces, and are especially relevant to estimating the surface radiative and energy budgets. The LSA SAF products are therefore expected to be relevant to a wide range of applications, including weather forecasting and climate modelling, renewable energy resource assessment, environmental management and land use, agricultural and forestry applications, and natural hazard management. In fact, the growing number of users in the latter topics together with the demands from environment monitoring and risk management communities (e.g., GMES requirements) supported the extension of biogeophysical parameters to wild fire related products (Trigo et al., 2009).

The LSA SAF is currently exploring (i) the capability of SEVIRI/MSG to detect and monitor active fires, particularly over Africa and Europe, leading to the operational generation, archiving and dissemination of the so-called Fire Detection and Monitoring (FD&M) product; and (ii) combining meteorological information with characteristics of vegetation to produce meaningful danger of fire rating for Southern Europe. In this respect the hereafter described Risk of Fire Mapping (RFM) product may be viewed as representing the first attempt to make an integrated use of meteorological information from meteorological forecasts, vegetation data from land cover maps and observations of active fires and fire pixels as obtained from the RFM product of the LSA SAF in order to produce coherent maps of fire risk at the scale of MSG.

The aim of the present document is to provide a detailed description of a contextual algorithm for detecting active fires, using information provided by MSG at the maximum temporal resolution (DaCamara et al., 2007; Amraoui et al., 2008). Section 2 gives a description of the adopted retrieval strategy as well as of the products to be delivered and of their relevant applications. Section 3 presents a thorough overview of the developed algorithm, hereafter referred to as FIre Detection ALGOrithm (FIDALGO) and describes the required inputs and the characteristics of the output data, focusing on results obtained during January 2007 over northern Africa, during July 2007 over southern Africa and during July-August of 2008 and 2009 over Europe. Validation of results is described in section 4, where maps of active fires as derived from FIDALGO are compared against independent data, namely those from the MODIS Fire Team.

1.2. Scope

This document describes the theoretical basis of the algorithms that generate the Fire Detection and Monitoring (FD&M) product.

2. Algorithm Overview

2.1. Retrieval Strategy

Depending on whether they are smouldering or flaming, most fires burn at temperatures between 500 and 1200 K (Dwyer et al., 2000b) but even higher temperatures (>1400 K) may occur in forested areas (Giglio et al., 1999). At these temperatures and in accordance with Planck's theory of blackbody radiation, there is a very strong emission in the middle-infrared (MIR) at wavelengths of 3-5 μm, as opposed to the background where the peaks of emission are located in the long-wave infrared (IR) at wavelengths of the order of 10 μm.

Most of the existing operational fire detection algorithms were developed for regional, continental and global applications and have been tuned accordingly. Generally speaking, the techniques utilize similar processing steps and input data (predominantly short- and long-wave IR bands) and the algorithms may be placed in two broad categories: fixed-threshold techniques and spatial analysis (or contextual) techniques (Justice and Dowty, 1994). Earlier algorithms of fire detection relied on static thresholds that were applied to the values recorded in MIR and IR channels. Appropriate values for the thresholds were computed empirically, depending on vegetation type, region and time of year.

More recent methods use contextual algorithms where values of thresholds are dynamically derived using appropriate statistics obtained from the neighbouring pixels. As pointed out by Flasse and Ceccato (1996), the main difference between contextual and fixed threshold algorithms is that a decision is made on a relative basis rather than on an absolute one; if the contrast between a given pixel and its surroundings is high enough then the pixel is identified as containing an active fire.

Contextual algorithms were first explored by Prins and Menzel (1992), using GOES data and by Justice et al. (1993) using AVHRR data. The approach was further

adopted for global and regional fire monitoring (Justice and Malingreau, 1996; Eva and Flasse, 1996; Dwyer et al., 1998; Stroppiana et al., 2000), and for the World Fire Web initiative (Grégoire et al., 2000). More recently, the contextual approach was used by the MODIS Fire Team to develop a global daily active fire product using MODIS data (Justice et al., 2002; Giglio et al., 2003a).

2.2. Delivered products

The aim of FIDALGO is to identify, every 15 minutes, MSG[1] pixels potentially contaminated with fires over the African and European continents. The list of fields given by the FD&M product is given in Annex A.

Detection and systematic monitoring of active fires over the African continent is essential for an accurate assessment of the overall fire activity, namely in protected areas e.g. national parks, reserves and hunting concessions. It also allows characterising the fire regimes in African protected areas and more specifically assessing their impacts on the natural habitats and consequently on the biodiversity.

Active fire detection over Europe is essential for early fire warning and for fire prevention, namely in what respects to a proper calibration of risk of fire indices, namely those that integrate the Risk of Fire Mapping (RFM) product currently being developed by the LSA SAF.

3. Algorithm Description

3.1. Theoretical Description

FIDALGO builds upon the above-mentioned contextual algorithms for AVHRR and MODIS. As schematically shown in Figure 1, the method consists of the following four main steps; 1) Pre-processing, 2) Selection of potential fire pixels, 3) Detection of contaminated pixels and 4) Confirmation of active fire pixels.

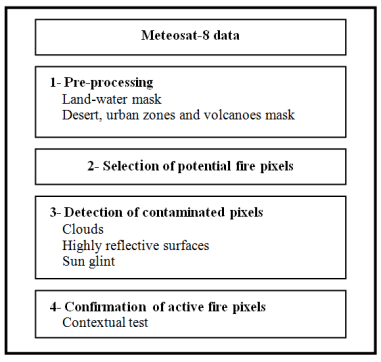

Figure 1. Schematic overview of the processing stages of FIDALGO.

[1] Meteosat Second Generation

Step 1 – Pre-processing

Surfaces such as exposed soil and rock are highly reflective at 3.9 μm, and may be the source of false fire detections. For instance, the algorithm by Arino et al. (1993) systematically identified large desert regions as very large burning areas, spanning thousands of pixels (Giglio et al., 1999; Mota et al., 2006).

A mask was accordingly defined that included pixels known to be associated with bare soils, inland water, volcanoes and urban zones. Land cover information from GLC2000 (Bartholomé and Belward, 2005) was used to generate a desert and water mask as well as to identify urban zones. Pixels contaminated by volcanoes were masked based on data from the Global Volcanism Program (http://www.volcano.si.edu). Figure 2 presents the defined mask over the African continent.

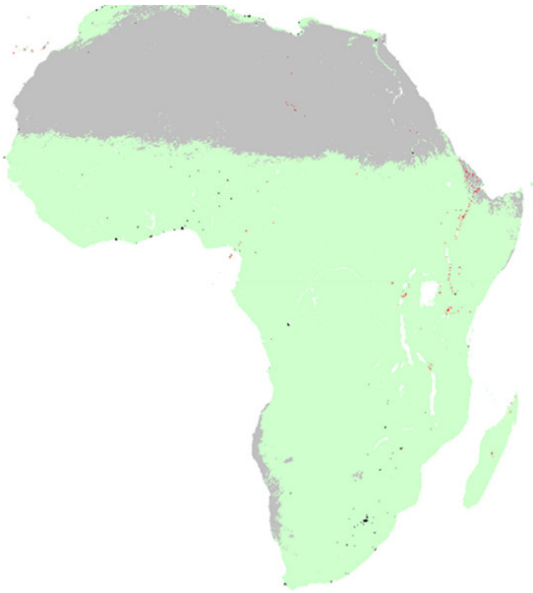

Figure 2. Mask of desert regions (grey pixels), inland water bodies (white pixels), urban zones (black pixels) and volcanoes (red pixels) over the African continent.

Step 2 – Selection of potential fire pixels

Selection of pixels likely to contain an active fire (Figure 3) may be achieved by simply applying, on a pixel-by-pixel basis, appropriate thresholds to MIR and to differences between MIR and IR channels (e.g., Arino et al., 1993; Flasse and Ceccato, 1996; Stroppiana et al., 2000; Justice et al., 2002; Giglio et al., 2003a,b).

Since the reflected MIR component increases with decreasing solar zenith angle, near solar noon a stronger reflected component may boost Tb(3.9) above the prescribed threshold leading to the detection of spurious fires. On the other hand, as the solar

component drops off with increasing solar zenith angle, some small fires may not pass the threshold test (Giglio et al., 1999). With the aim of mitigating commission (omission) errors for low (high) solar zenith angles (SZA), during day time (i.e. for SZA<85°) thresholds imposed by FIDALGO both on Tb(3.9) and on differences ΔT=Tb(3.9)-Tb(10.8) vary throughout the day. Accordingly, a pixel is considered as containing a potential fire if one of the following conditions is fulfilled:

$$\begin{aligned}
&Tb(3.9)\geq 315K \text{ and } \Delta T\geq 10K \text{ for } SZA<70^\circ \\
&Tb(3.9)\geq 313K \text{ and } \Delta T\geq 9K \text{ for } 70^\circ\leq SZA<73^\circ \\
&Tb(3.9)\geq 311K \text{ and } \Delta T\geq 7K \text{ for } 73^\circ\leq SZA<76^\circ \\
&Tb(3.9)\geq 309K \text{ and } \Delta T\geq 5K \text{ for } 76^\circ\leq SZA<79^\circ \\
&Tb(3.9)\geq 307K \text{ and } \Delta T\geq 4K \text{ for } 79^\circ\leq SZA<82^\circ \\
&Tb(3.9)\geq 306K \text{ and } \Delta T\geq 3K \text{ for } 82^\circ\leq SZA<85^\circ
\end{aligned} \qquad (1a)$$

During night time (i.e. for SZA≥85°), a potential fire is attributed to a given pixel if the following condition holds:

$$Tb(3.9)\geq 305K \text{ and } \Delta T\geq 3K \text{ for } SZA\geq 85^\circ \qquad (1b)$$

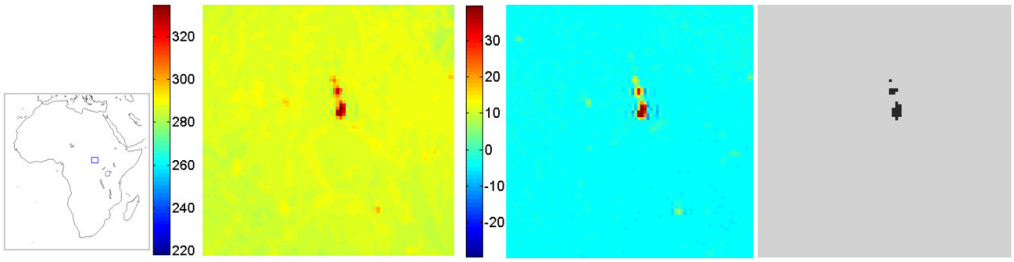

Figure 3. An example of fire pixels as identified over a selected region in the African continent using information from the Meteosat image obtained by SEVIRI at 23:00 UTC of 23/01/2007. a) map of Africa where the location of the region is indicated by the small rectangular frame; b) values (in K) of Tb(3.9) according to the colour bar on the left; c) values (in K)of ΔT=Tb(3.9)-Tb(10.8) according to the colour bar on the left; d) location of confirmed vegetation fires (pixels in black) by FIDALGO (see Step 4 of the algorithm).

Step 3 – Detection of contaminated pixels

Contamination of channel 3.9 μm by clouds is the most commonly occurring source of false alarms during daytime. When illuminated by sunlight, clouds typically appear as regions of elevated Tb(3.9) (due to reflected sunlight) and of reduced Tb(10.8) (due to their cooler temperatures), leading to a net increase in ΔT that may give rise to an erroneous detection of pixels affected by active fires.

Several cloud identification techniques may be employed, ranging in quality from simple (e.g. spatially fixed thresholds) to highly sophisticated (inter-active analyst-controlled) ones. The following two extreme situations may result; (1) excessive cloud detection, which inadvertently masks fires, smoke and large cloud-free areas; (2) failure to mask most small and some large clouds, causing many false alarms (Giglio et al., 1999).

Cloud detection by FIDALGO is based on a simplified version of Saunders and Kriebel (1988) algorithm. A given day time pixel is considered as cloud or contaminated by clouds, and therefore eliminated, if one of the following three conditions is fulfilled, i.e.

$$R(0.6)+R(0.8)>1.2$$

or

$$Tb(12.0)<265K \quad (2a)$$

or

$$R(0.6)+R(0.8)>0.8 \text{ and } Tb(12.0)<285K$$

During night time, pixels are flagged as cloud if the following condition is satisfied:

$$Tb(12.0)<265K \quad (2b)$$

Since SEVIRI channel IR3.9 covers parts of both the solar and thermal ranges of the electromagnetic spectrum, it is crucial to reject those pixels whose values in the IR3.9 channel would be too high (or even saturate) due to high reflection, rather than high temperature (Flasse and Ceccato, 1996).

Accordingly, a given pixel is considered as representing a highly reflective surface and therefore eliminated if the following condition (Giglio et al., 1999) is fulfilled during daytime:

$$R(0.8)>0.25 \quad (3)$$

For certain sun-earth-satellite configurations false fire detections may occur due to specular reflexion of sunlight by water bodies, wet soils, cirrus clouds, cloud edges and, in rare instances, by bare soils (Stroppiana et al., 2000; Giglio et al., 2003a).

A given pixel is considered contaminated by sunglint, and therefore eliminated, if i) its neighbouring pixels are water bodies, sparsely vegetated or bare soils or contaminated by clouds and ii) the following condition is fulfilled during daytime:

$$SZA>40° \text{ and } R(0.8)>0.20 \quad (4)$$

Examples of detection of contaminated pixels (clouds, highly reflective surfaces and areas of sunglint) are shown in Figure 4.

Step 4 – Confirmation of active fire pixels

A potential fire pixel is confirmed as a pixel containing an active fire by comparing its spectral signature against the radiative properties of the respective background (Kaufman and Justice 1998). The background is defined as a 5×5 pixel grid centred at the potential fire pixel and valid background pixels are all those that i) were neither masked in step 3 nor identified as potential fire pixels in step 2 and ii) fulfill the following conditions:

$$Tb(3.9)\geq 312K \text{ and } \Delta T\geq 10K \text{ for } SZA<70°$$

$$Tb(3.9)\geq 310K \text{ and } \Delta T\geq 9K \text{ for } 70°\leq SZA<73°$$

$$Tb(3.9)\geq 308K \text{ and } \Delta T\geq 7K \text{ for } 73°\leq SZA<76° \quad (5a)$$

Tb(3.9)≥306K and ΔT≥ 5K for 76°≤SZA<79°

Tb(3.9)≥304K and ΔT≥ 4K for 79°≤SZA<82°

Tb(3.9)≥303K and ΔT≥ 3K for 82°≤SZA<85°

during day time, or the following condition:

Tb(3.9)≥302K and ΔT≥3K for SZA≥85° (5b)

during night time.

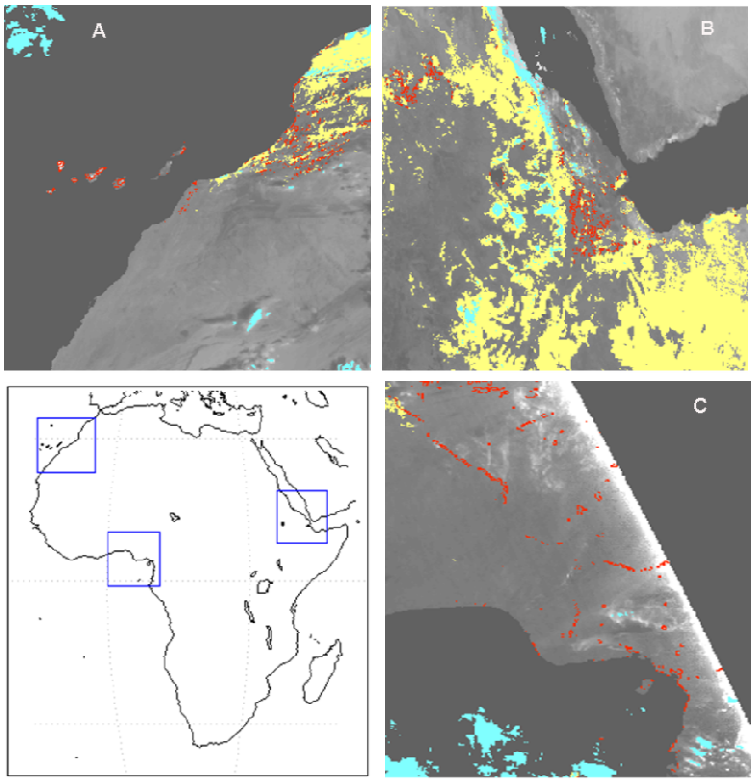

Figure 4. Examples of contaminated pixels as identified in three selected regions in the African continent whose locations are given by the rectangular frames in the map of Africa (lower left panel). Images correspond to SEVIRI R(0.8) as obtained at 08:00 UTC of 23/01/2007 (A), 11:15 UTC of 22/01/2007 (B) and 17:15 UTC of 23/01/2007 (C). Pixels in cyan, in yellow and in red respectively indicate clouds, highly reflective surfaces and areas of sunglint.

Valid background pixels are then used to compute a set of statistics that characterise the background (Giglio et al., 1999), namely the mean and the absolute mean deviation of $\mathrm{Tb}(3.9)$, respectively denoted as $\overline{\mathrm{Tb}}(3.9)$ and $\delta(3.9)$:

$$\overline{\mathrm{Tb}}(3.9) = \frac{1}{N}\sum_{i=1}^{N} \mathrm{Tb}_i(3.9) \quad (6a)$$

$$\delta(3.9) = \frac{1}{N}\sum_{i=1}^{N} \left|\mathrm{Tb}_i(3.9) - \overline{\mathrm{Tb}}(3.9)\right| \quad (6b)$$

as well as the mean and absolute mean deviation of ΔT, respectively denoted as $\overline{\Delta T}$ and $\delta(\Delta T)$:

$$\overline{\Delta T} = \frac{1}{N}\sum_{i=1}^{N} \Delta T_i \quad (7a)$$

$$\delta(\Delta T) = \frac{1}{N}\sum_{i=1}^{N} |\Delta T_i - \overline{\Delta T}| \quad (7b)$$

The number of valid neighbouring pixels in the grid must be at least three, *i.e.* $N \geq 3$. If there is an insufficient number of valid surrounding pixels, statistics are not computed and the pixel is kept classified as potentially containing a fire.

A potential fire pixel is finally confirmed as a pixel containing an active fire when the two following conditions are met (Giglio et al., 1999):

$$\mathrm{Tb}_{PF}(3.9) > \overline{\mathrm{Tb}}(3.9) + \delta(3.9) - 3$$
$$\text{and} \quad (8a)$$
$$\Delta T_{PF} > \overline{\Delta T} + \max(2.5 * \delta(\Delta T), 4)$$

during daytime, or the following condition:

$$\Delta T_{PF} > \overline{\Delta T} + \max(2.5 * \delta(\Delta T), 4) \quad (8b)$$

is fulfilled during night time. It may be noted that the subscript PF in the equations (8a) and (8b) indicates values corresponding to the potential fire pixel.

Figure 5 presents an example of potential pixels that were confirmed by FIDALGO as containing active fires. In this case, the presence of active fires may be visually validated because of the conspicuous presence in the same locations of rising smoke plumes.

3.2. Practical considerations

3.2.1. Input data

There are two kinds of input data required to properly run the algorithm:

i) static data, which are delivered and updated by the developers of the FD&M algorithm;
ii) dynamic data, which are generated during the pre-processing phase at every time step.

3.2.1.1. Static data

One of the required static data is a file with the geographical location (longitude and latitude) of all volcanoes in a specific region (see Figure 2).

The other static file is the GLC2000 land cover provided in the MSG projection for the specified regions in HDF5 format.

3.2.1.2. Dynamic data

As shown in Table 1, remotely-sensed information consists of top of the atmosphere (TOA) radiances of SEVIRI/Meteosat-8 at the maximal temporal resolution (i.e. every 15 minutes) for the following bands; visible channels centred at 0.635 µm (VIS0.6) and 0.81 µm (VIS0.8) and infrared channels centred at 3.92 µm (IR3.9), 10.8 µm (IR10.8) and 12.0 µm (IR12.0). TOA visible radiances from VIS0.6 and VIS0.8 were converted into reflectances, respectively referred to hereafter as R(0.6) and R(0.8). TOA infrared radiances from channels IR3.9, IR10.8 and IR12.0 were in turn converted into brightness temperatures, respectively denoted hereafter as Tb(3.9), Tb(10.8) and Tb(12.0). For each pixel and time-step, FIDALGO also makes use of the respective solar zenith angle.

Table 1. SEVIRI channels used in FIDALGO.

Channel	Purpose
R(0.6)	Cloud detection
R(0.8)	Cloud detection, bright surface and sunglint detection
Tb(3.9)	Active fire detection
Tb(10.8)	Active fire detection
Tb(12.0)	Cloud detection

3.2.2. Modes of operation and exception handling

The algorithm may run in two modes of operation for a specific geographical region and date, the difference relying in the way channel IR039 is ingested in the algorithm ,i.e. either in the form of brightness temperature or in the for of channel radiance.

The geographical areas allowed by the algorithm are presented in Table 2. They are defined by the respective name and the corners position, relative to an MSG image of 3712 columns per 3712 lines, starting from North to South and from West to East.

Table 2 - Characteristics of geographical areas to process algorithm.

Region Name	Description	Initial Column	Final Column	Initial Line	Final Line	Size in Columns	Size in Lines	Total Number of Pixels
NAfr	Northern Africa	1240	3450	700	1850	2211	1151	2.544.861
SAfr	Southern Africa	2140	3350	1850	3040	1211	1191	1.442.301
EUR	Europe	463	2163	3013	3663	1701	651	1 107 351

When input values for a given pixel are not physically acceptable then a set of filters (Table 3) is applied to the input data to mask out all in this context. The filters are applied to the reflectances of channels VIS006 and VIS008 (Ref006 and Ref008) and to either the radiance or the brightness temperature of channel IR039 depending on the mode of operation.

Table 3 – Input data filters.

Variable	Condition	Assigned Value
Rad039	≤0	0.01
Tb039	<0	-9999
Ref006	≥2	1
Ref006	<-1	-1
Ref008	≥2	1
Ref008	<-1	-1

3.2.3. Output data

The procedure allowed identifying both active fires (i.e. occurrences in a given pixel of a given image) and fire pixels (i.e. pixels where at least one active fire was detected). Identified fire pixels were further classified into the following three categories;

- Single occurrence fires defined as active fires that are isolated events in space and time, i.e. having occurred only once in the entire period and with no active fires identified in the neighbouring pixels neither in the same image nor in the previous and the following ones;
- Fires over sparse herbaceous or sparse shrub cover, defined as active fires occurring over pixels classified as belonging to GLC2000 class 14 (Table 1 and Figure 1);
- Vegetation fires which include all active fires that do not belong to the previous categories.

As shown in Table 4, a grand total of 370 239 (325 923) active fires were detected, distributed over 73 046 (73 863) fire pixels within the NAfr (SAfr) window, during January (July) 2007. Single occurrences account for about 5% of active fires in both windows and fires over sparse herbaceous or sparse shrub cover represent about 2.5% in NAfr, being negligible in SAfr.

Table 4. Active fires and fire pixels over NAfr and SAfr windows during January and July 2007, respectively.

	NAfr	SAfr
Vegetation fires	341801	310771
Single occurrence	19581	15132
Sparse herb./shrub.	8857	20
Active fires	370239	325923
Fire pixels	73046	73863

Figure 5 presents the spatial distribution of identified active fires and fire pixels. Most burning activity over NAfr may be found in the Sahel region, especially in southern Chad, the Central African Republic, southern Sudan and in various regions of West Africa, with the exception of Nigeria, which displays lower fire density. Burning activity over SAfr is concentrated in northern Angola, the southern Democratic Republic of Congo and eastern Zambia.

Table 5 presents the distribution of vegetation fires among the different GLC2000 land cover classes. In both NAfr and SAfr windows, two classes clearly dominate: “Tree cover, broadleaved, deciduous, open”, containing 40 % of total fires observed, and “Shrub cover, closed-open, deciduous”, with 25 % of total fires in NAfr and 19 % in SAfr. It may be also noted that more than two-thirds (70%) of fires in SAfr were observed in GLC2000 classes dominated by trees (i.e. “Tree cover, broadleaved, evergreen”, “Tree cover, broadleaved, closed” and “Tree cover, broadleaved, deciduous, open”, in contrast with NAfr where the proportion is much lower (40%).

Ninety percent of NAfr fires concentrate in just four vegetation classes (bold, Table 5), namely “Tree cover, broadleaved, deciduous, open”, “Shrub cover, closed-open, deciduous”, “Mosaic: tree cover/other natural vegetation” and “Mosaic: cropland/shrub or grass cover”, respectively accounting for 40%, 25%, 17% and 8% of total fires. In SAfr, 93% of active fires also concentrate in four vegetation classes (bold, Table 5), namely “Tree cover, broadleaved, deciduous, open”, “Tree cover, broadleaved, closed”, “Shrub cover, closed-open, deciduous” and “Herbaceous cover, closed-open”, respectively accounting for 40%, 25%, 19% and 9% of total fires. There are two remarkable differences between the two hemispheres: whereas the “Tree cover, broadleaved, closed” class contains 25% of SAfr fires, this class is fire-free in NAfr. Conversely, the class “Mosaic: tree cover/other natural vegetation” encompasses 17% of all NAfr fires, but is unaffected in SAfr.

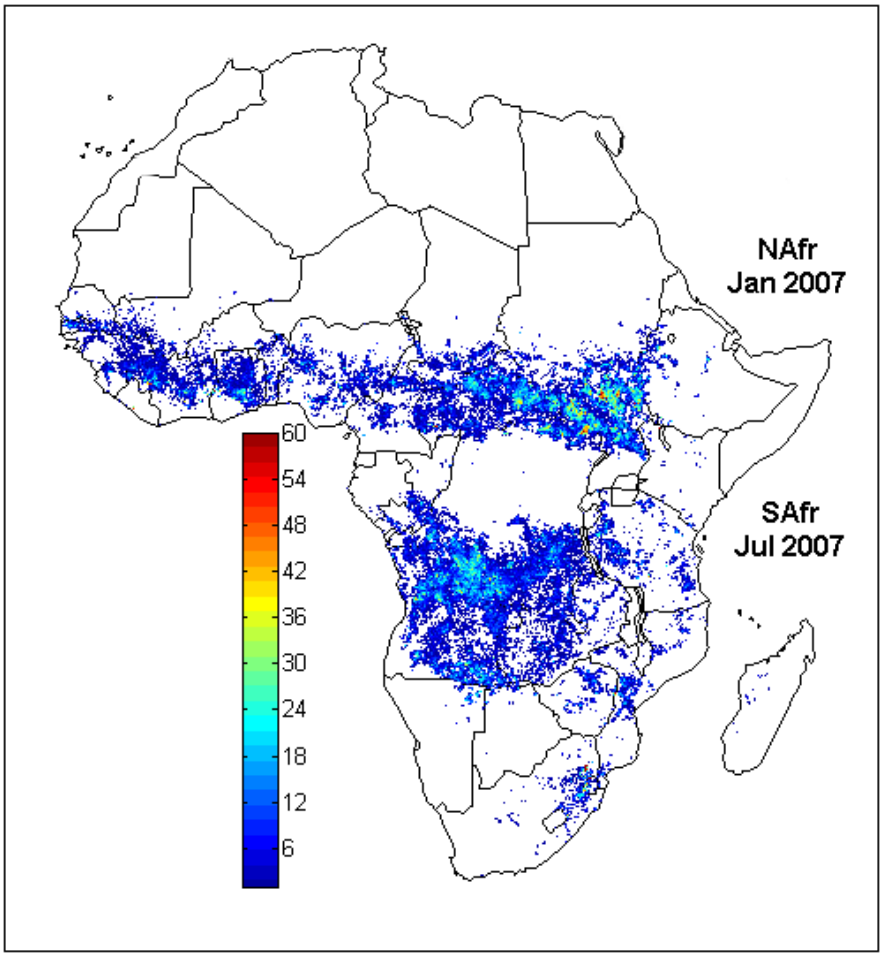

Figure 5. Fire pixels over NAfr and SAfr windows, respectively during January and July 2007. The colour bar indicates for each fire pixel the number of identified active fires.

Table 5. Distribution of active fires among the different of GLC2000 land cover classes for NAfr and SAfr during January and July 2007, respectively.

Code	Land cover type	NAfr (%)	SAfr (%)
1	Tree cover, broadleaved, evergreen	1	4
2	Tree cover, broadleaved, closed	0	**25**
3	Tree cover, broadleaved, deciduous, open	**40**	**40**
7	Tree cover, regularly flooded, fresh water	0	0
8	Tree cover, regularly flooded, saline water	0	0
9	Mosaic: tree cover/other natural vegetation	**17**	0
12	Shrub cover, closed-open, deciduous	**25**	**19**
13	Herbaceous cover, closed-open	3	**9**
15	Regularly flooded shrub and/or herbaceous cover	2	0
16	Cultivated and managed areas	1	3
17	Mosaic: cropland/tree cover/other natural vegetation	3	0
18	Mosaic: cropland/shrub or grass cover	**8**	0

It is worth pointing out that the observed fire incidence by land cover class compares well with the results of Barbosa et al. (1999) and Tansey et al. (2004a,b). The former authors used White's Vegetation of Africa map (White, 1983), and found that over 50% of the area burned, detected during the period 1982-1991, was located in three vegetation types, designated "Undifferentiated Ethiopian, Sudanian, and North Zambezian woodland", "Sudanian woodland with abundant Isoberlinia", and "Mosaic of Guineo-Congolian Lowland Forest and Secondary Grassland". An additional 20% of area burned affected "Wetter Zambezian Woodland Miombo", "Somalia-Masai Acacia-Commiphora Deciduous Bushland and Thicket", and "Drier Zambezian Miombo Woodland". Therefore, areas of open tree cover (*i.e.*, woodlands) are also found to be the vegetation type most affected by fire. Plate 3 of Barbosa et al. (1999) shows the location of the six most fire-prone African vegetation types, confirming the good match with our findings.

In their analysis of global area burned during the year 2000, Tansey et al. (2004a,b) identified the Northern Hemisphere sub-tropical shrubland and wooded grassland belt in Africa (with the exception of Somalia and Nigeria) as the region with the greatest burning activity per surface area in the world. In southern hemisphere Africa, peaks of burned area density were found in northern Angola and the southern Democratic Republic of Congo, also concurring with our own results.

Table 6 and Figure 6 provide information about fire activity during summer (defined as July + August) of 2008 and 2009. It is worth noting that, in 2009, although there are less fire pixels (3414) than in 2008 (3734) the larger duration observed (18866 in 2009 versus 11791 in 2008) provides an indication that summer 2009 was a more severe season in terms of fire duration and therefore in terms of burned area.

The spatial distribution of fire pixels and active fires clearly shows regions of high activity namely Portugal, Spain, southern France, Italy, Greece, Turkey, Croatia, Serbia, Romania, Bulgaria and Ukraine.

Table 6. As in Table 4 but respecting to the EUR window during July-August 2008 and 2009.

	Europe 2008	Europe 2009
Active fires	11791	18866
Fire pixels	3734	3414

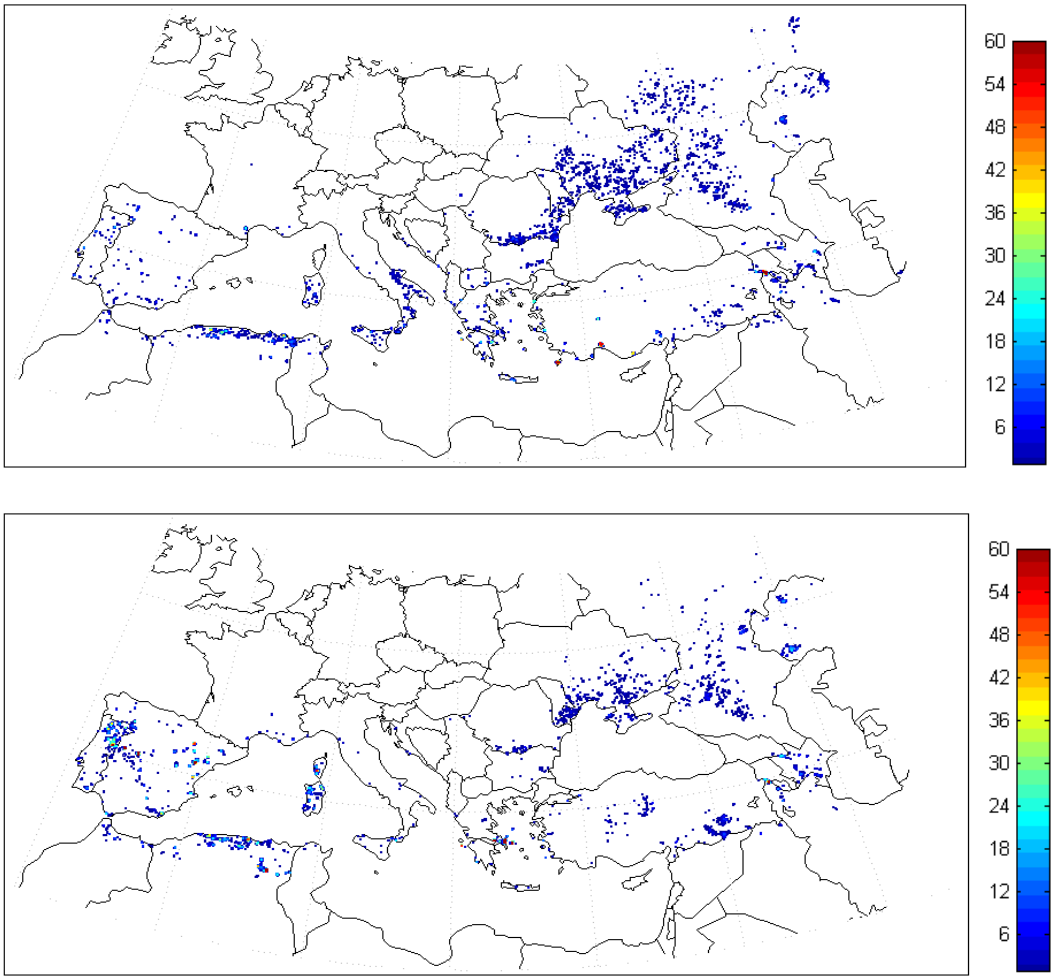

Figure 6. As in Figure 5 but respecting to active fires and fire pixels in the EUR window during July August 2008 (upper panel) and July-August 2009 (lower panel).

4. Product Validation

4.1. Rationale

In the case of detection and monitoring of active vegetation fires, any validation procedure involves checking at least the following two key aspects of the developed detection algorithm; i) whether it is sensitive, minimizing omission errors, and ii) whether it is selective, minimizing commission errors or false alarms. Concerning sensitiveness, it is worth mentioning that, according to Calle et al. (2006), SEVIRI is able to detect fires of less than 1 ha in size, with a fire temperature higher than 600 K. In what regards commission errors, it is worth emphasizing that FIDALGO includes several tests aiming to detect and eliminate false alarms.

Validation of the FD&M product was performed by comparing results obtained with FIDALGO against those from the global daily active fire product developed by the MODIS Fire Team (Justice et al., 2002). In this respect, it may be noted that when

comparing results obtained from geostationary sensors, such as SEVIRI, with those from polar-orbit sensors, such as MODIS, the spatial and the temporal resolutions of the instruments are the two main factors that have to be accounted for. Moreover, when the comparison involves data from polar sensors with finer spatial resolution, the procedure is especially complex due to errors caused by data misregistration (Calle et al., 2008).

The FD&M product is based on information from SEVIRI on-board Meteosat-8. This sensor provides a very high temporal resolution (*i.e.* images with a 15-minute repeat cycle) but the spatial resolution is low, corresponding to 3×3 km^2 at the sub-satellite point (SSP) and decreasing with increasing distance from SSP.

The MODIS active fire data consist of hot spots as detected by the MODIS radiometer on-board the polar-orbiting Terra and Aqua platforms. The MODIS fire detection algorithm is based on a contextual algorithm developed by Giglio et al. (2003a). Information is obtained from thermal channels at coarse spatial resolution (*i.e.* with a pixel size of the order of 1×1 km^2) and with a low temporal resolution consisting of four observations per day (Justice et al., 2002) and corresponding to the maximum temporal resolution of the above mentioned radiometer. The MODIS active fire data is part of the MODIS Fire Products that include an identification of the occurrence of thermal anomalies, as well as estimates of the total emitted power from the fire and of the burned area.

An operational procedure that allows dealing with the problem posed by the different spatial and temporal scales of geostationary and polar orbiting instruments was proposed by Calle et al. (2008). Their study covered the region of Galicia (Spain) spanning a period of intense fire activity, from the 1st to the 20th of August 2006. The authors relied on remotely sensed data from three different sensors; SEVIRI on-board Meteosat-8, MODIS on-board Terra and Aqua, and AWifs on-board Resourcesat-1.

The procedure proposed by Calle et al. (2008) consisted of dividing the region in squared blocks with length L × L and then building up a linear model of active fire counts as obtained using SEVIRI in each block versus the counts obtained in the same block when using a different sensor. Calle et al. 2008 have shown that the coefficient of determination, ρ^2, linearly increased with the logarithm of L, *i.e.* according to the law $\rho^2 = \alpha + \beta \ln(L)$, where α and β are constants.

In the present study the procedure by Calle et al. (2008) is generalised to the time domain, *i.e.* the study area and period will be subdivided in space-time blocks of N SEVIRI pixels × N SEVIRI pixels × T days and linear models will be derived that relate fire counts over each block as obtained from FIDALGO with corresponding numbers from the MODIS active fire database. An extended law relating ρ^2 with ln(N) and ln(T) will also be investigated, *i.e.* the coefficient of determination is estimated according to the linear model:

$$\rho^2 = c + a\ \ln(N) + b\ \ln(T) \qquad (9a)$$

where a, b and c are constants to be determined.

It is worth noting that the above equation may be rewritten in the form of the following power law:

$$\exp(\rho^2) = C \times N^a \times T^b \qquad (9b)$$

where $C=e^c$.

4.2. Comparison with the MODIS active fire product

As shown in Figure 7 two regions were selected in the African continent, one within NAfr and the other within SAfr windows. Both regions have the same size (192 × 192 SEVIRI pixels) and cover areas of intense fire activity. The period of study spans one month in both selected regions, namely January and July 2007 for the regions within NAfr and SAfr, respectively.

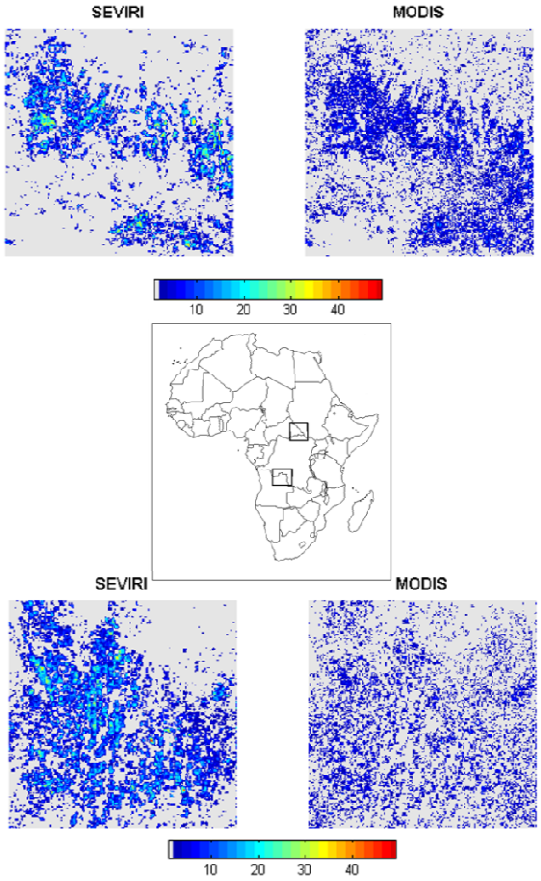

Figure 7. Fire pixels detected over the two selected regions of 192 ×192 pixels, one within the NAfr window (upper panels) and the other within SAfr (lower panels) during January and July 2007, respectively. The two small rectangular regions in the map of Africa (central panel) indicate the geographical location of the selected regions. Left (right) panels display fire counts as obtained from SEVIRI using FIDALGO (from the MODIS active fire data base). For each fire pixel, the colour bar indicates the number of identified active fires.

Results obtained reflect the different spatial and temporal characteristics of the MODIS and SEVIRI instruments. Whereas the number of fire pixels identified in the MODIS active database is much larger than those in the FD&M product, the number of

identified active fires is by far greater in the latter case. This is to be expected taking into account the finer spatial resolution of MODIS and the higher frequency of SEVIRI.

The different features of the results obtained with the FD&M and MODIS products suggest investigating the relationship between fire counts as obtained from MODIS and from SEVIRI as well as the dependency of such relationship on the adopted spatial and temporal scales. The two selected areas were accordingly subdivided in blocks of N SEVIRI pixels × N SEVIRI pixels × T days for different combinations of N and T. Fire counts as obtained from FIDALGO were then related with those obtained from MODIS by means of linear models and the respective coefficients of determination, ρ^2, were used as a measure of fitness.

Linear models of the type described by Equations (8a) and (8b) were used to characterize the dependency of coefficients of determination on the spatial scale N and the temporal scale T. The two following linear models were obtained:

$$\rho^2 = 0.02 + 0.21\ln(N) + 0.07\ln(T) \qquad (10a)$$

for the region inside NAfr and

$$\rho^2 = -0.02 + 0.17\ln(N) + 0.07\ln(T) \qquad (10b)$$

for the region inside SAfr. Both models are shown in Figure 8 and their adequacy to describe the dependency of ρ^2 on N and T is worth being noted, given the high values of the obtained correlation coefficients, respectively 0.95 and 0.96 for the linear models defined over the regions inside NAfr and SAfr.

The similarity between the models obtained for the two regions is striking, especially in what respects to dependency with ln(T), where the coefficient of 0.07 is the same in both models. The increase of ρ^2 with ln(N) is larger than the one with ln(T), being slightly greater in the case of the region inside NAfr, a feature that may be attributed to differences between the two regions in what respects to landscape and land cover, as well as to number of fire pixels and of active fires.

Obtained results point out the fact that a given explained variance may be achieved by using models based on different pairs of N and T. Choice of specific values of explained variance ρ^2, spatial scale N and temporal scale T will then depend on the purpose of the study to be undertaken. Table 7 and Figure 8 present examples of results obtained based on three different combinations of N and T, all of them leading to linear models characterised by values of $\rho^2 \approx 0.64$.

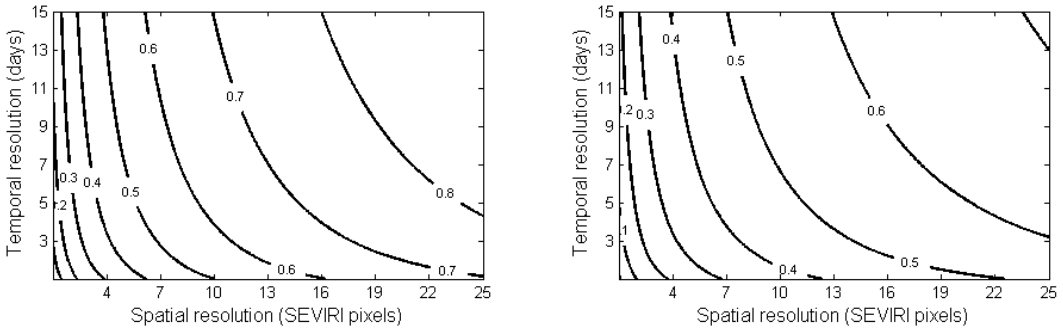

Figure 8. Dependency on spatial resolution (in SEVIRI pixels) and time resolution (in days) of the coefficient of determination (ρ^2) of linear models relating number of active fires obtained from the FD&M product versus those obtained from the MODIS active fire database, respectively over the selected regions of 192 × 192 SEVIRI pixels within NAfr (left panel) and SAfr (right panel) windows.

Table 7. Three examples of linear models defined over the selected window within NAfr that relate the number of active fires as obtained from the MODIS active fire database (y_{MODIS}) with the number of active fires as obtained from the FD&M product (x_{SEVIRI}). M, b and ρ respectively denote the slope, the intercept and the correlation coefficient of each linear model whereas B, S and RMSE respectively denote the bias, the standard deviation and the root mean square of errors, e (defined as $x_{SEVIRI} - y_{MODIS}$).

N×N pixels – T days	Number of pixels	$y_{MODIS} = m \times x_{SEVIRI} + b$			$e = x_{SEVIRI} - y_{MODIS}$		
		M	bt	P	B	S.	RMSE
6×6 pixels – 10 days	2 695	0.30	11.73	0.79	8.95	50.28	51.06
8×8 pixels – 6 days	2 567	0.30	12.31	0.81	9.39	56.53	57.30
12×12 pixels – 3 days	2 135	0.28	15.12	0.78	10.89	63.36	64.29

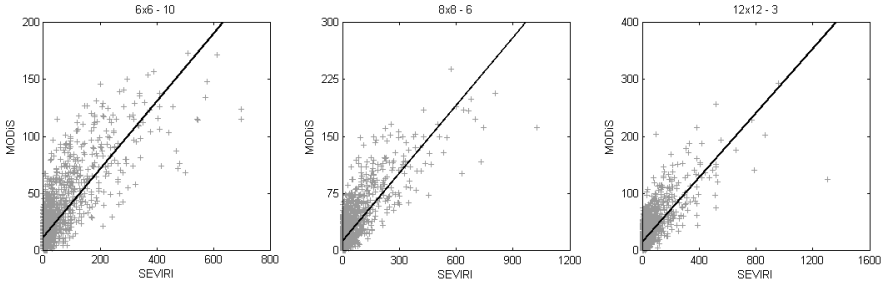

Figure 9. Dispersion diagrams and regression lines respecting to the three linear models described in Table 6. It may be noted that different scales (in both axes) were used in the figures.

It may be observed that the characteristics of the three models are very similar. For blocks containing small amounts of active fires the FD&M product will indicate lower values than the MODIS product. This feature, which translates into the positive values of the intercept and the low value (much less than 1) of the slope, is clearly related to the low spatial resolution of the SEVIRI instrument. However, in the case of blocks containing high amounts of active fires the FD&M product will indicate much higher values than the MODIS product. This is clearly related with the much higher frequency of the SEVIRI instrument and reflects on the obtained positive values of bias B (Table 6). Finally it may be noted that the mean square error, $(RMSE)^2$, is almost entirely due to random errors; in fact, the variance, in all models represents 97% of the mean square error, S^2, the square of the bias, B^2, representing the remaining 3%.

5. References

Amraoui, M., DaCamara, C.C., & Pereira, J.M.C. (2008). Fire detection and monitoring over Africa. 2008 EUMETSAT Meteorological Satellite Conference, Darmstadt, Germany, 08 - 12 September. EUMETSAT P.52, ISBN 978-92-9110-082-8.

Andreae, M.O. and P. Merlet. (2001). Emission of trace gases and aerosols from biomass burning. *Global Biogeochemical Cycles*, *15*, 955-966, 2000GB001382.

Andreae, M.O., D. Rosenfeld, P. Artaxo, A.A. Costa, G.P. Frank, K.M. Longo and M.A.F. Silva-Dias, (2004). Smoking rain clouds over the Amazon. *Science*, *303*, 1337-1342.

Arino, O., J.-M. Melinotte and G. Calabresi (1993). Fire, cloud, land, water: the "Ionia" AVHRR CD-Browser of ESRIN. EOQ 41, ESA, EST EC, Noordwijk, July 1993.

Barbosa, P.M., D. Stroppiana, J.-M. Grégoire, and J.M.C. Pereira (1999). An assessment of vegetation fire in Africa (1981-1991): burned areas, burned biomass, and atmospheric emissions. *Global Biogeochemical Cycles 13*, 933-950.

Bartholomé, E. and A.S. Belward (2005). GLC2000: A new approach to global land cover mapping from Earth observation data. *International Journal of Remote Sensing, 26*, 1959-1977.

Cahoon, D.R., B.J. Stocks, J.S. Levine, W.R. Cofer and K.P. O'Neill (1992). Seasonal distribution of African savanna fires. *Nature, 359*, 812-815.

Calle, A., J.L. Casanova and A. Romo (2006). Fire detection and monitoring using MSG Spinning Enhanced visible and Infrared Imager (SEVIRI) data. *Journal of Geophysical Research*, *111*, G04S06, doi: 10.1029/2005JG000116G04S06.

Calle A., F. Gonzalez-Alonso, and S. Merino de Miguel (2008). Validation of active forest fires detected by MSG-SEVIRI by means of MODIS hot spots and AWiFS images. *International Journal of Remote Sensing*, Vol. 29, 3407-3415.

Cihlar J., A. Belward and Y. Govaerts (1999). Meteosat Second Generation opportunities for land surface research and applications. EUMETSAT Scientific Publications EUM SP 01.

Csiszar I., L. Denis, L. Giglio, C.O. Justice and J. Hewson (2005). Global fire activity from two years of MODIS data. *International Journal of Wildland Fire*, 14, 117-130, doi: 10.1071/WF03078.

DaCamara C.C. (2006). The Land Surface Analysis SAF: one year of pre-operational activity. The 2006 EUMETSAT Meteorological Satellite Conference, Helsinki, Finland, 12-16 June 2006, EUMETSAT P.48, ISBN 92-9110-076-5, 8pp. (available from http://www.eumetsat.int/Home/Main/Publications/index.htm).

DaCamara C.C., Calado, T.J., Amraoui, M., and Pereira, J.M.C (2007). The SAF for Land Surface Analysis: wildfire applications. 2007 EUMETSAT Meteorological Satellite Conference and the 15th Satellite Meteorology & Oceanography Conference of the American Meteorological Society, Amsterdam, Netherlands, 24 - 28 September. EUMETSAT P.50, ISBN 92-9110-079-X.

Desanker P.V., P.G.H. Frost, C.O. Justice and R.J. Scholes (Eds.) (1997). The Miombo network: framework for a terrestrial transect study of land-use and land-cover change in Miombo ecosystems of Central Africa. IGBP Report 41, The International Geosphere-Biosphere Programme (IGBP), Stockholm, Sweden, 190 pages.

Dwyer E., J.-M. Grégoire and J.P. Malingreau (1998). A global analysis of vegetation fires using satellite images: spatial and temporal dynamics. *Ambio*, 27, pp. 175-181.

Dwyer, E., J.M.C. Pereira, J.-.M. Grégoire and C.C. DaCamara (1999). Characterization of the spatio-temporal patterns of global fire activity using satellite imagery for the period April 1992 to March 1993, Journal of Biogeography, 27 (1), 57-69 (DOI: 10.1046/j.1365-2699.2000.00339.x).

Dwyer E., J.-M. Grégoire and J.M.C. Pereira (2000a). Climate and vegetation as driving factors in global fire activity. In *Biomass burning and its inter-relationships with the climate system*, edited by J.L. Innes, M. Beniston and M.M. Verstraete, pp. 171-191, Springer, New York.

Dwyer E., S. Pinnock, J.-M. Grégoire and J.M.C. Pereira (2000b). Global spatial and temporal distribution of vegetation fire as determined from satellite observations. *International Journal of Remote Sensing*, Vol. 21, No. 6, pp. 1289-1302.

Eck T.F., B.N. Holben, D.E. Ward, M.M Mukelabai, O. Dubovik, A. Smirnov, J.S. Schafer, N.C. Hsu, S.J. Piketh, A. Queface, J. Le Roux, R.J. Swap and I. Slutsker (2003). Variability of biomass burning aerosol optical characteristics in Southern Africa during the SAFARI 2000 dry season campaign and a comparison of single scattering albedo estimates from radiometric measurements. *Journal of Geophysical Research*, Vol. 108, 8477, doi:10.1029/2002JD002321.

Eva H. and S. Flasse (1996). Contextual and multi-threshold algorithms for regional active fire detection with AVHRR data. *Remote Sensing Reviews*, Vol. 14, pp. 333-351.

Flasse S.P. and P. Ceccato (1996). A contextual algorithm for AVHRR fire detection. *International Journal of Remote Sensing*, Vol. 17, No. 2, pp. 419-424.

Frost P.G.H. (1999). Fire in Southern African woodlands origins, impacts, effects, and control. In Proceeding of an FAO Meeting on Public Policies Affecting Forest Fires, FAO Forestry Paper 138, pp. 181-205.

Galanter M., H. Levy II and G.R. Carmichael (2000). Impacts of biomass burning on tropospheric CO, NO_x and O_3. *Journal of Geophysical Research*, Vol. 105, pp. 6633-6653.

Garstang M. and P.D. Tyson (1997). Atmospheric circulation, vertical structure and transport over Southern Africa during the SAFARI-92 campaign. In *Fire in Southern Africa Savannas: Ecological and Atmospheric Perspectives* (B.W. van Wilgen, M.O. Andreae, J.G. Goldammer and J.A. Lindesay, Eds.), pp. 57-88. Witwatersrand University Press, Johannesburg, South Africa.

Generoso S., F.-M. Balkanski, O. Boucher and M. Schulz (2003). Improving the seasonal cycle and interannual variations of biomass burning aerosol sources. *Atmos. Chem. Phys.*, 3, pp. 1211-1222.

Giglio L., J.D. Kendall and C.O. Justice (1999). Evaluation of global fire detection algorithms using simulated AVHRR infrared data. *International Journal of Remote Sensing*, Vol. 20, No. 10, pp. 1947-1985.

Giglio L., J. Descloitres, C.O. Justice and Y.J. Kaufman (2003a). An enhanced contextual fire detection algorithm for MODIS. *Remote Sensing of Environment*, Vol. 87, pp. 273-282.

Giglio L., D. Kendall and R Mack (2003b). A multi-year active fire dataset for the tropics derived from the TRMM VIRS. *International Journal of Remote Sensing*, Vol. 24, No. 22, pp. 4505-4525.

Giglio L., I. Csiszar and C.O. Justice (2006). Global distribution and seasonality of active fires as observed with the Terra and Aqua Moderate Resolution Imaging Spectroradiometer (MODIS) sensors. *Journal of Geophysical Research*, Vol. 111, G02016, doi:10.1029/2005JG000142.

Giglio L. (2007). Characterization of the tropical diurnal fire cycle using VIRS and MODIS observations. *Remote Sensing of Environment*, Vol. 108(4), pp. 407-421.

Grégoire J.-M., D.R. Cahoon, D. Stroppiana, S. Pinnock, H. Eva, O. Arino, J.M. Rosaz and I. Csiszar (2000). Forest fire monitoring and mapping for GOFC: current products and information networks based on NOAA-AVHRR, ERS-ATSR and SPOT-VGT systems. Forest Fire Monitoring and Mapping: A component of Global Observation of Forest Cover. Italy: Joint Research Centre, Ispra, pp. 111-135.

Hoffer A., A. Gelencsér, M. Blazsó, P. Guyon, P. Artaxo and M.O. Andreae (2006). Diel and seasonal variations in the chemical composition of biomass burning aerosol. *Atmos. Chem. Phys.*, 6, pp. 3505-3515.

Ito, A. and J.E. Penner (2004). Global estimates of biomass burning emissions based on satellite imagery for the year 2000. *Journal of Geophysical Research*, Vol. 109, D14S05, doi:10.1029/2003JD004423

Justice C.O., J.P. Malingreau and A.W. Setzer (1993). Satellite remote sensing of fires: potential and limitations. *Fire in the Environment: the Ecological Atmospheric, and Climatic Importance of Vegetation Fires*, edited by P.J. Crutzen and J.G. Goldammer (New York: J. Wiley and Sons), pp. 77-88.

Justice C.O. and P. Dowty (1994). IGBP-DIS satellite fire detection algorithm workshop technical report. *IGBP-DIS Working Paper 9*, NASA/GSFC, Greenbelt; Maryland; USA.

Justice C.O. and J.P. Malingreau (editors) (1996). The IGBP-DIS fire algorithm workshop 2. IGBP-DIS Working Paper 14, Ispra Italy, October 1995.

Justice C.O., L. Giglio, S. Korontzi, J. Owens, J.T. Morisette, D. Roy, J. Descloitres, S. Alleaume, F. Petitcolin and Y. Kaufman (2002). The MODIS fire products. *Remote Sensing of Environment*, Vol. 83, pp. 244-262.

Kendall J.D., C.O. Justice, P.R. Dowty, C.D. Elvidge and J.G. Goldammer (1997). Remote Sensing of Fires in Southern Africa During the SAFARI 1992 Campaign. In *Fire in Southern African Savannas*, B. van Wilgen, M. Andreae, J. Goldammer and J.A. Lindesay (Eds), pp. 89-133 (Johannesburg: Witwatersrand University Press).

Lacaux J.-P., H. Cachier and R. Delmas (1993). Biomass burning in Africa: an overview of its impact on atmospheric chemistry. In: *Fire in the Environment: The Ecological, Atmospheic, and Climatic Importance of Vegetation Fires*. Ed. P.J. Crutzen and J.G. Goldammer, J.Wiley and Sons,Chichester, UK.

Le Page, Y., J.M.C. Pereira, R.M. Trigo, C.C. DaCamara, D. Oom and B. Mota (2008). Global fire activity patterns (1996-2006) and climatic influence: an analysis using the World Fire Atlas, Atmos. Chem. Phys., 8, 1911-1924.

Mota B., J.M.C. Pereira, D. Oom, M.J.P. Vasconcelos and M. Schultz (2006). Screening the ESA ATSR-2 World Fire Atlas (1997-2002). *Atmospheric Chemistry and Physics*, Vol. 6: 1409-1424.

Pereira J.M.C. and Y. Govaerts (2001). Potential fire applications from MSG/SEVIRI observations. EUMETSAT Programme Development Department, Technical Memorandum No. 7.

Prins E.M. and W.P. Menzel (1992). Geostationary satellite detection of biomass burning in Southern America. *International Journal of Remote Sensing*, Vol. 13, pp. 2783-2799.

Prins E.M. and W.P. Menzel (1994). Trends in South American biomass burning detected with the GOES VAS from 1983-1991. *Journal of Geophysical Research*, 99 (D8), pp. 16719-16735.

Prins E.M., and J. Schmetz (2000). Diurnal active fire detection using a suite of international geostationary satellites. In *Forest Fire Monitoring and Mapping: A Component of Global Observation of Forest Cover*, (F. Ahern, J.-M. Grégoire and C. Justice, eds.), pp.139-148. European Commission Joint Research Centre, EUR19588EN.

Roberts G., M.J. Wooster, G.L.W. Perry, N. Drake, L-M. Rebelo and F. Dipotso (2005). Retrieval of biomass combustion rates and totals from fire radiative power observations:

application to southern Africa using geostationary SEVIRI Imagery. *Journal of Geophysical Research* 110, D21111: doi: 10.1029/2005JD006018.

Roberts G.J. and M.J. Wooster (2008). Fire detection and fire characterization over Africa using Meteosat SEVIRI. *IEEE Transactions on Geoscience and Remote Sensing*, Vol. 46, No. 4, pp. 1200-1218.

Rosenfeld, D. (1999). TRMM observed first direct evidence of smoke from forest fires inhibiting rainfall. *Geophysical Research Letters*, 26 (20), pp. 3105-3108.

Saunders R.W. and K.T. Kriebel (1988). An improved method for detecting clear sky and cloud radiances from AVHRR data. *International Journal of Remote Sensing*, Vol. 9, pp. 123-150.

Schmetz J., P. Pili, S. Tjemkes, D. Just, J. Kerkmann, S. Rota and A. Ratier (2002). An introduction to Meteosat Second Generation (MSG), Bulletin of the American Meteorological Society 83 (7), pp. 977–992 doi:10.1175/1520-0477(2002)083

Schultz M.G. (2002). On the use of ATSR fire count data to estimate the seasonal and interannual variability of vegetation fire emissions. *Atmos. Chem. Phys.*, 2, pp. 387-395.

Schultz, M.G., A. Heil, J.J. Hoelzemann, A. Spessa, K. Thonicke, J.G. Goldammer, A.C. Held, J.M.C. Pereira, and M. van het Bolscher (2008). Global wildland fire emissions from 1960 to 2000. *Global Biogeochemical Cycles*, Vol. 22, GB2002, doi:10.1029/2007GB003031

Silva J.M.N., J.M.C. Pereira, A.I. Cabral, A.C.L. Sá, M.J.P. Vasconcelos, B. Mota and J.-M. Grégoire (2003). An estimate of area burned in Southern Africa during the 2000 dry season using SPOT-VEGETATION satellite data. *Journal of Geophysical Research*, Vol. 108, 8498, doi:10.1029/2002JD002320.

Smirnov A., B.N. Holben, T.F. Eck, I. Slutsker, B. Chatenet and R.T. Pinker (2002). Diurnal variability of aerosol optical depth observed at AERONET (Aerosol Robotic Network) sites. *Geophysical Research Letters*, 29 (23), 2115, doi:10.1029/2002GL016305.

Stroppiana D., S. Pinnock and J.-M. Grégoire (2000). The global fire product: daily fire occurrence from April 1992 to December 1993 derived from NOAA AVHRR data. *International Journal of Remote Sensing*, Vol. 21, No. 6, pp. 1279-1288.

Tansey K.J., J.-M. Grégoire, D. Stroppiana, A. Sousa, J. Silva, J.M.C. Pereira, L. Boschetti, M. Maggi, P. Brivio, R. Fraser, S. Flasse, D. Ershov, E.Binaghi, D. Graetz and P. Peduzzi (2004a). Vegetation burning in the year 2000: global burned area estimates from SPOT VEGETATION data. *Journal of Geophysical Research*, doi:10.1029/2003JD003598.

Tansey, K., J-M. Grégoire, E. Binaghi, L. Boschetti, P.A. Brivio, D. Ershov, S. Flasse, R. Fraser, D. Graetz, M. Maggi, P. Peduzzi, J.M.C. Pereira, J. Silva, A. Sousa e D. Stroppiana (2004b). A global inventory of burned areas at 1 km resolution for the year 2000 derived from SPOT VEGETATION data. *Climatic Change* 67: 345–377.

Trigo I., DaCamara, C., Viterbo, P., Roujean, J.L., Olesen, F., Barroso, C., Camacho-de Coca, F., Carrer, D., Freitas, S., García-Haro, F., Geiger, B., Gellens-

Meulenberghs, F., Meliá, J., Ghilain, N., Pessanha, L., Siljamo, N. and Arboleda, A., 2009: The Satellite Application Facility on Land Surface Analysis. *Int. J.Rem Sens.* (in press).

van Wilgen B.W. and R.J. Scholes (1997). The vegetation and fire regimes of Southern-hemisphere Africa. In BW van Wilgen, MO Andreae, JG Goldammer, and JA Lindesay (Eds.) *Fire in Southern African Savannas: Ecological and Atmospheric Perspectives*, pp. 27-46. Witwatersrand University Press, Johannesburg, South Africa.

White, F. (1983). The vegetation of Africa, a descriptive memoir to accompany the UNESCO/AETFAT/UNSO vegetation map of Africa. UNESCO, Natural resources research, XX, 356 pp.

ANNEX A

At each time step the FD&M algorithm generates two external output files with: 1) FD&M classification (Table 8) and 2) the metadata, according to the following name convention:

1) **HDF5_LSASAF_MSG_FDeM_<Area>_YYYYMMDDHHMM**

and

2) **HDF5_LSASAF_MSG_FDeM-METADATA_<Area>_YYYYMMDDHHMM**

where **<Area>**, **YYYY**, **MM**, **DD**, **HH** and **MM** denote the geographical region (see Table 2), the year, the month, the day, the hour and the minute of data acquisition, respectively.

FD&M product is provided in the HDF5 format as requested by the LSA-SAF system. This format allows defining a set of attributes that provide the relevant information.

Table 8. Description of FD&M classification.

# Class	Description
1	Water
2	Land
3	Land with fire

An additional metadata file provides information about several relevant variables (**Error! Reference source not found.** and Table 11) for the pixels, if any, identified with i) sun glint, ii) high reflectivity, iii) confirmed and iv) not confirmed fires. This file includes one matrix dataset for each one of these items where columns correspond to the relevant variables and the lines correspond to the occurrence. The name of each dataset in the HDF5 file is pointed out in **Error! Reference source not found.**. If none of these items is detected, the output file is composed only by the general attributes [RD.1] and no datasets are included. The datasets ELEM_HR, ELEM_SG and ELEM_NC are only written if the "`minimize_metadata`" flag is turned OFF (=0). All attributes of the metadata file are described in the **Error! Reference source not found.**.

Table 9. Names and description of dataset that composes the output metadata files of FD&M.

Dataset Name	Description
ELEM_HR	Pixel ELEMents identified with High Reflectivity
ELEM_SG	Pixel ELEMents identified with Sun Glint
ELEM_CF	Pixel ELEMents with a Confirmed Fire
ELEM_NC	Pixel ELEMents with a Non Confirmed Fire

Table 10. Description of variables in the datasets ELEM_HR, ELEM_SG and ELEM_NC.

# Column	Variable Description
1	Line of the pixel identified as high reflectivity, sun glint or non-confirmed fire
2	Column of the pixel identified as high reflectivity, sun glint or non-confirmed fire
3	Reflectivity of SEVIRI channel VIS006 [Adim.]
4	Reflectivity of SEVIRI channel VIS008 [Adim.]
5	Brightness temperature of SEVIRI channel IR039 [K]
6	Difference of brightness temperatures IR039 – IR108 [K]
7	Satellite zenith angle [º]
8	Brightness temperature of SEVIRI channel IR108 [K]
9	Brightness temperature of SEVIRI channel IR120 [K]

Table 11 - Description of variables in the dataset ELEM_CF.

# Column	Variable Description
1	Line of the pixel identified as a confirmed fire
2	Column of the pixel identified as a confirmed fire
5	Brightness temperature of SEVIRI channel IR039 [K]
6	Difference of brightness temperatures IR039 – IR108 [K]
7	Satellite zenith angle [º]
3	Reflectivity of SEVIRI channel VIS006 []
4	Reflectivity of SEVIRI channel VIS008 []
8	Brightness temperature of SEVIRI channel IR108 [K]
9	Brightness temperature of SEVIRI channel IR120 [K]